

Nonclassical wave propagation measurements in the high temperature vapor of D6 with the asymmetric shock tube for experiments in rarefaction waves (ASTER)

Chandrasekaran, Nitish; Michelis, Theodoros; Mercier, Bertrand; Falsetti, Chiara; Colonna, Piero

DOI

[10.1007/s00348-024-03843-8](https://doi.org/10.1007/s00348-024-03843-8)

Publication date

2024

Document Version

Final published version

Published in

Experiments in Fluids

Citation (APA)

Chandrasekaran, N., Michelis, T., Mercier, B., Falsetti, C., & Colonna, P. (2024). Nonclassical wave propagation measurements in the high temperature vapor of D6 with the asymmetric shock tube for experiments in rarefaction waves (ASTER). *Experiments in Fluids*, 65(7), Article 111. <https://doi.org/10.1007/s00348-024-03843-8>

Important note

To cite this publication, please use the final published version (if applicable). Please check the document version above.

Copyright

Other than for strictly personal use, it is not permitted to download, forward or distribute the text or part of it, without the consent of the author(s) and/or copyright holder(s), unless the work is under an open content license such as Creative Commons.

Takedown policy

Please contact us and provide details if you believe this document breaches copyrights. We will remove access to the work immediately and investigate your claim.



Nonclassical wave propagation measurements in the high temperature vapor of D_6 with the asymmetric shock tube for experiments in rarefaction waves (ASTER)

Nitish Chandrasekaran¹ · Theodoros Michelis¹ · Bertrand Mercier² · Chiara Falsetti¹ · Piero Colonna¹

Received: 12 April 2024 / Revised: 20 June 2024 / Accepted: 21 June 2024 / Published online: 11 July 2024
© The Author(s) 2024

Abstract

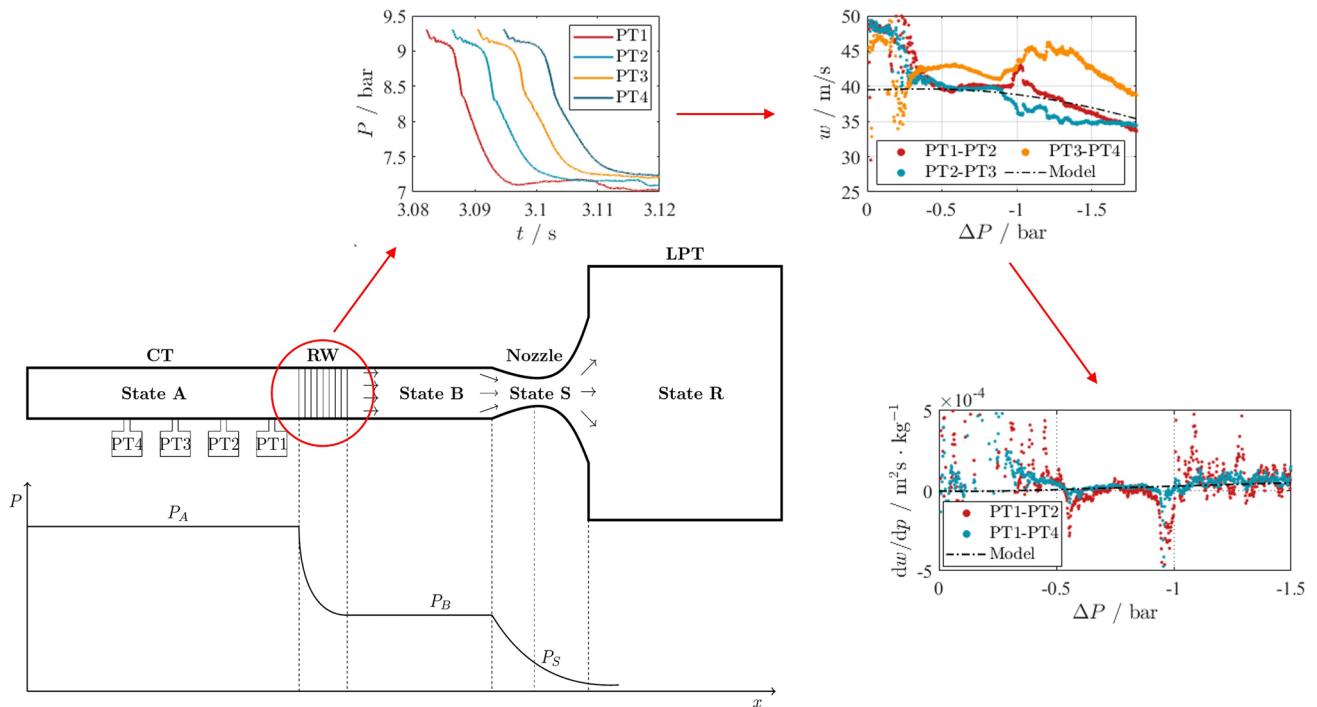
A novel test setup called the asymmetric shock tube for experiments on nonideal rarefaction waves (ASTER) has been commissioned at Delft University of Technology. The ASTER, which works according to the principle of Ludwig tubes, is designed to generate and measure the speed of small and finite amplitude waves propagating in the dense vapors of fluids formed by complex organic molecules, therefore in the nonideal compressible fluid dynamics regime. The ultimate goal of the associated research is to prove the existence of nonclassical gasdynamics. The setup consists of a high-pressure charge tube and a vacuum tank separated by a glass disk equipped with a breaking mechanism for rarefaction waves experiments. When the glass disk is broken, an expansion wave propagates into the tube in the direction opposite to the fluid flow. The propagation speed of this wave is measured using a time-of-flight method with the help of four fast-response pressure sensors placed equidistantly in the middle of the tube. The charge tube can withstand pressures and temperatures of up to 15 bar and 400°C. Preliminary rarefaction experiments were successfully conducted using dodecamethylcyclohexasiloxane, D_6 , as the working fluid and at pressures and temperatures of up to 9.4 bar and 372°C, respectively. The results of an experiment featuring the initial state for which a theoretical model predicts the nonclassical acceleration of rarefaction waves show that the propagation is qualitatively different from that put into evidence by experiments for which the propagation is classic. Upcoming setup improvements and experimental campaigns are planned with the objective of experimentally verifying the existence of nonclassical gasdynamics.

✉ Chiara Falsetti
c.falsetti@tudelft.nl

¹ Propulsion & Power, Delft University of Technology,
Kluyverweg 1, 2629HS Delft, Zuid-Holland,
The Netherlands

² Institut P', CNRS, Univ. de Poitiers, ISAE-ENSMA - UPR
3346, SP2MI, Poitiers, France

Graphical abstract



1 Introduction

Nonideal compressible fluid dynamics (NICFD), and nonclassical gasdynamics within it, is the branch of fluid mechanics concerned with flows of fluids whose thermodynamic and transport properties are nonideal, i.e., their relation is more complex than that mathematically described by the ideal gas model (Guardone et al. 2024). One of the consequences is that in these flows, also the sound speed varies differently from how it varies in ideal gas flows. Nonideal single-phase thermodynamic states occur for states that are close to the vapor-liquid critical point (dense vapor and supercritical fluid) for which, therefore, the compressibility factor $Z = \frac{pv}{RT} \neq 1$, where p is the pressure, v is the specific volume, T the temperature and R the specific gas constant.

Compressible flow features depend on the variation of the speed of sound; therefore, the late professor Thompson introduced a thermodynamic property, the fundamental derivative of gasdynamics (Thompson 1971)

$$\Gamma = 1 + \frac{\rho}{c} \left(\frac{\partial c}{\partial \rho} \right)_s, \tag{1}$$

to initiate and develop the theoretical treatment of this class of flows. In Eq. (1), c is the speed of sound, ρ is the density and s is the entropy. In the case of ideal gases, Γ is constant

and equal to $(\gamma + 1)/2$, where $\gamma = c_p/c_v$ is the ratio of specific heats.

If a molecule is sufficiently complex (sufficiently large specific heat), Γ is lower than 1 for a finite set of nonideal vapor thermodynamic states (e.g., for states defined by a range of pressures and temperatures) and in flows of fluids in these states, c may vary in the opposite way compared to how it varies in an ideal gas flow. Therefore, it decreases upon compression and increases upon rarefaction. These fluid flows are qualitatively similar to ideal gas flows, but quantitatively different.

The illustrious scientists Hans Bethe and Yakov Zel'dovich were the first to speculate, independently from one another, that nonclassical phenomena, i.e., rarefaction shock waves (RSW) and compression fans are theoretically possible if the specific heat of the substance in the involved thermodynamic states is sufficiently large. Thompson then showed that if Γ is lower than zero, nonclassical gasdynamics may occur, and several complex organic molecules were identified as fluids whose flows may display such exotic features. They are termed Bethe-Zel'dovich-Thompson (BZT) fluids.

The reader is referred to the recent review article of Guardone et al. (2024) for the theoretical treatment of NICFD and an overview of its applications. More extensive information regarding nonclassical gasdynamics, both its theoretical

developments and experimental attempts to prove its existence, can be found in, e.g., the Ph.D. dissertations of Nannan (2009), Head (2021), and Chandrasekaran (2023).

The existence of a thermodynamic region with negative nonlinearity and the formation of RSWs have been extensively studied from a theoretical standpoint. However, only a few experimental attempts have been made to prove their existence, and they too have provided only inconclusive results. The first shock tube experiments aimed at generating and detecting a RSW were conducted by Borisov et al. (1983), who claimed to have observed a propagating rarefaction shock wave in the single-phase dense vapor of Freon-13 (trichlorofluoromethane, CClF_3). However, these results have been confuted by several authors, see, e.g., the treatment of Nannan et al. (2013), who proposed as an explanation of the observed expansion shock wave that the measured pressure profiles are related to the expansion of a condensing fluid, given that the molecule of Freon-13 is too simple for any vapor state to feature $\Gamma < 0$.

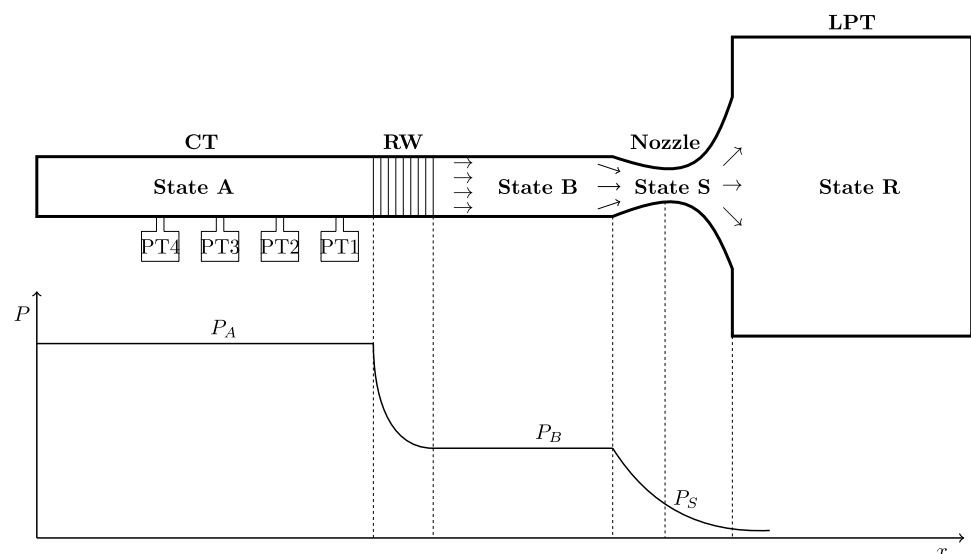
A second shock tube experiment with the same objective was attempted by Ferguson (2001) at the University of Colorado at Boulder. The researcher chose PP10 (perfluorofluorene, $\text{C}_{13}\text{F}_{22}$) as the test fluid. Unfortunately, the experiment failed because of the thermal decomposition of the fluid at the high temperature of the test conditions. Moreover, the lack of accurate information on the thermodynamic properties of the fluid would have prevented the estimation of the sound speed with sufficient accuracy to demonstrate that the observed expansion was indeed supersonic (Guardone et al. 2009).

The most recent attempt to generate and measure a RSW propagating in the single-phase dense vapor of a fluid made of complex organic molecules was performed using the flexible asymmetric shock tube (FAST) at the Delft University of Technology by Mathijssen et al. (2015). Unlike

the earlier experiments which relied on a shock tube where a diaphragm separated the high from the low-pressure sections of the device, the FAST employed a fast opening valve (FOV), which in principle offered the advantage of the more repeatable opening of the barrier element and of performing consecutive tests without the need for opening the fluid enclosure to replace the diaphragm. The researchers reported performing several measurements in which the initial thermodynamic state of the fluid (a siloxane, dodecamethylcyclohexasiloxane, D_6) featured $\Gamma < 0$ according to the best available thermodynamic models, and documented evidence of the possibility of RSWs forming in the expanding flow (Mathijssen 2017). However, the FOV, a rather complex device, suffered from numerous mechanical problems owing to the high operating temperatures, which is possibly the most challenging aspect of this kind of experiments. Moreover, measurements of the internal wall temperature of the FAST performed afterwards by the authors of this article showed large gradients in the axial direction. Since Γ is very sensitive to temperature variations (Chandrasekaran et al. 2021), these measurements suggest that those earlier experiments were in conditions whereby so-called mixed classical/nonclassical wave formed (Chandrasekaran 2023).

This article presents the commissioning of the asymmetric shock tube for experiments on nonideal rarefaction waves (ASTER) and results from the preliminary experiments aimed at measuring rarefaction wave propagation using D_6 as working fluid. Figure 1 shows the rather simple working principle of the ASTER experiment. The setup consists of two major components, namely the charge tube (CT) and the low pressure tank (LPT). The CT and the LPT are connected to each other through a nozzle section. The CT contains the vapor of the working fluid at the set pressure and temperature. A glass-disk diaphragm placed at the exit of the nozzle separates the high pressure vapor in the CT

Fig. 1 Schematic representation of an ASTER experiment, together with the qualitative pressure variation with time that pressure transducers along the charge tube (PT1, PT2, PT3, PT4) can measure



from the LPT which is under vacuum. When the glass-disk is broken, a rarefaction wave (RW) propagates into the CT, reducing the pressure in the CT from State A to State B and generating a flow through the nozzle (see Fig. 1). Sonic conditions (State S) are achieved in the nozzle throat. If the pressure waves accelerate, they eventually coalesce into a rarefaction shock wave, which travels at a speed which is greater than the speed of sound at the thermodynamic state of the quiescent fluid.

Another challenge of the study of nonclassical flows is the poor accuracy of the existing thermodynamic models of BZT fluids. While so-called technical equations of state models have been developed for several of these fluids, see, e.g., the work of Colonna et al. (2008), their accuracy is much lower if compared to models of fluid made of simpler molecules due to the lack of accurate property measurements, especially for nonideal states. One of the reasons, apart from the fact that their industrial use is less common, is that nonideal states are at high temperatures (of the order of 250 to 350°C); thus, any accurate measurement is extremely difficult. Aiming at improving thermodynamic models, the authors of this article recently measured the speed of sound of siloxane D_6 with the fluid in dense vapor states (Mercier et al. 2023), therefore at high temperature, close to the thermal stability threshold.

A definitive proof that nonclassical gasdynamic phenomena can be generated and measured is still missing, and the setup described here, together with its characterization and first experiments, are motivated by the wish of providing such experimental evidence. An overview of the experimental setup is presented in Sect. 2: it provides details on the components of the facility and on the control and data acquisition system. Section 3 presents the results of the characterization of the setup demonstrating the correct operation of the facility. Results of the preliminary rarefaction wave measurements in the test fluid D_6 are reported in Sect. 4.

Section 5 highlights the concluding remarks and outlines future work.

2 The setup

The ASTER is a Ludwieg-type tube (or asymmetric shock tube) recently designed and built at Delft University of Technology and its design benefits from the lesson learned by operating the FAST (Mathijssen 2017). Figure 2 shows a simplified CAD drawing of the ASTER, while Fig. 3 displays a photograph of the realized setup. A schematic layout is reported in Fig. 4.

The CT is a 3 m long stainless steel tube with an outside diameter of 35 mm and a thickness of 2.35 mm. The heating of the CT is achieved through two 1250 W glass-silk heating jackets each with a 25 mm layer of insulation. Any longitudinal variation in the performances of the heating system may result in axial temperature gradients along the CT. These gradients can have a significant effect on the formation and propagation of rarefaction waves in the CT (Chandrasekaran et al. 2021). To avoid temperature variations along the tube, the stainless steel inner tube of the CT is covered with eight semi-cylindrical aluminum shells, each 750 mm long, 35 mm in outer radius and 17.5 mm thick. This promotes a uniform temperature distribution along the setup due to the higher thermal conductivity of aluminum (see Chandrasekaran 2023, Chapter 3). The CT assembly is placed on sliding supports to allow for its thermal expansion at high temperatures, which is approximately 20 mm at 400°C.

The other end of the CT is connected to the Low Pressure Tank (LPT) which is kept at vacuum at the beginning of a test. The LPT is a 4.5 L stainless steel cylinder with an internal length of 338 mm, an outside radius of 69.5 mm, and a thickness of 4 mm. It is heated using a 300 W glass-silk jacket with a 25 mm insulation layer. The blanket only

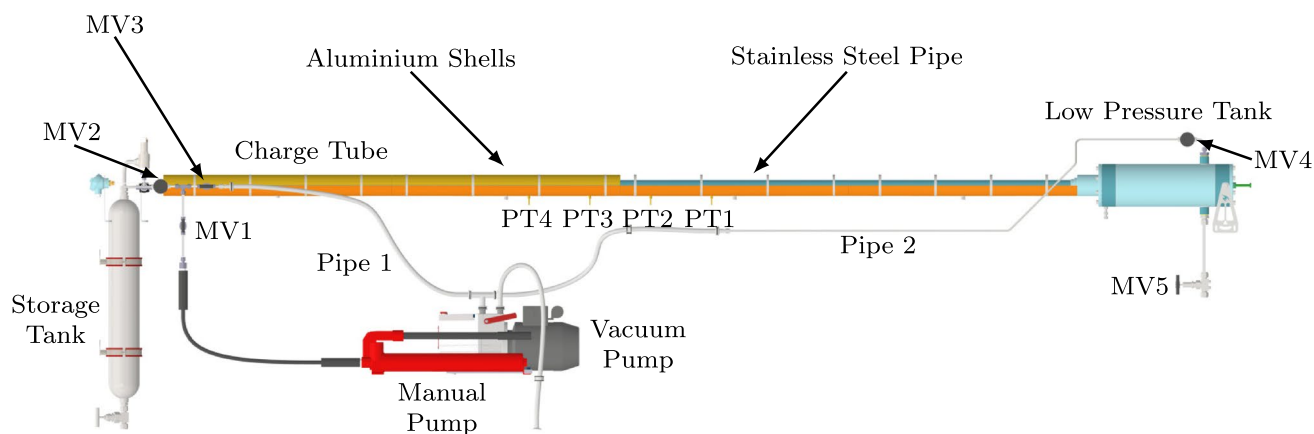


Fig. 2 Simplified CAD drawing of the ASTER setup

partially covers the LPT to make way for piping connections at the end of the vessel. The CT and the LPT are connected via a nozzle section. The nozzle creates a throat area to choke the flow, thereby preventing flow disturbances in the LPT from travelling upstream into the CT.

A glass disk placed at the exit of the nozzle separates the CT and the LPT, and acts as the barrier element. The expansion of the high-pressure vapor in the CT into the LPT is achieved by breaking the glass disk with a manually actuated mechanism. The ASTER uses a glass-disk diaphragm due to its simplicity and envisaged reliability. Conventional metallic or Mylar® diaphragm designs generally rely on the pressure difference across the diaphragm to achieve a complete opening, see, e.g., the works of Tranter et al. (2001); Houas et al. (2003); Furukawa et al. (2007); Nambiar et al. (2017). Nonclassical gasdynamic experiments feature lower pressure differences across the barrier element if compared to more common shock tube experiments. Such low pressure difference likely results in an incomplete opening of

the diaphragm, which has a strong impact on the formation of a shock wave (Gaetani et al. 2008). Glass, on the other hand, breaks instantaneously once a crack is initiated thereby ensuring a complete and almost instantaneous opening.

2.1 Instrumentation, data acquisition and control

A NI cDAQ 9189 chassis is the core of the sensors measurement and control system. It can accommodate 8 input/output modules for analog or digital signals. The chassis is connected via ethernet to a computer for experiment monitoring, and data acquisition and storage. The NI modules used for data acquisition, along with the instrument they are connected to, are listed in Table 1. NI LabView is used for monitoring and programming/executing the control functions.

Temperature is the only controlled variable. The temperatures along the CT are measured using eight 1 mm thick K-type thermocouples (TCs) placed equidistantly in the aluminum shells. The tips of the TCs are housed inside

Fig. 3 Photograph of the ASTER setup. The charge tube and the low pressure tank are covered with glass-silk heating jackets



Fig. 4 General layout of the ASTER

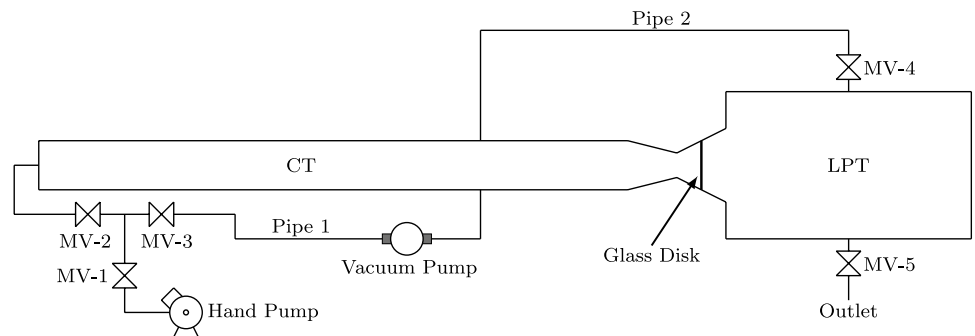


Table 1 Input and output modules installed in the National Instruments CompactDAQ 9189 chassis for data acquisition, monitoring and control

Model	Type	Range	Channels	Instrument(s)
NI9264	Voltage output	0–10 V	16	Thyristors
NI9222	Voltage input	0–10 V	4	Dynamic pressure sensors
NI9203	Current input	4–20 mA	8	Static pressure sensor
NI9124	Temperature input	–	16	Thermocouples
NI9217	Temperature input	–	4	PT100

grooves drilled into the shells such that they lie within a few millimeters of the contact surface between the aluminum and the stainless steel. This ensures that the TCs provide a good estimate of the temperature at the surface of the CT and are not affected by the local wall temperature close to the blankets (see Fig. 5). Each blanket covers four TCs, and the average temperature of these four TCs is used as the process variable for the PID control of the corresponding blanket.

The temperature of the LPT is measured using the PT100 that is integrated into the thermal blanket. The vessel is heated to the same setpoint as the CT in order to minimize temperature gradients across the nozzle. A schematic of the temperature control system is shown in Fig. 6. The thermal energy supply to the facility is regulated using a PID control implemented in the *ASTER_vi* program. The voltage to the heating elements is supplied by a RKC single-phase thyristor (THV-1PZ-020-5*NN-6).

PT100 sensors are located in the thermal blankets covering the CT too, but their measurements are used only for monitoring purposes and are not a part of the control

system. The temperature of the working fluid inside the CT is measured using a stand-alone PT100 sensor placed at the inlet-side end, as shown in Fig. 7. To prevent leaking of the working fluid through the probe connections, the PT100 is not placed in direct contact with the fluid. Instead, it is housed in a 135 mm long stainless steel thermowell that protrudes into the CT and is welded onto the CT endplate. The thermocouples and the stand-alone PT100 sensor are calibrated with a Fluke 9100 S dry-well calibrator with a rated accuracy of ± 0.5 K.

The static pressure of the fluid in the CT is measured by a Druck UNIK 5000 ref. X5072-TB-A2-CA-H1-PA sensor with a specified accuracy of $\pm 0.1\%$ over the full range of 16 bar. This sensor, however, is rated for a maximum temperature of only 125°C and is therefore mounted on the inlet pipe connecting MV2 and the CT (see Fig. 7), away from direct contact with the hot vapor. A safety release valve rated for 16 bar is also fitted at the location to prevent any unexpected surge in the fluid pressure. The outlet



Fig. 5 Thermocouple attached to the aluminum shell in the ASTER. The thermocouples are placed within a heat resistant fabric sheath to prevent damage to the heating blankets

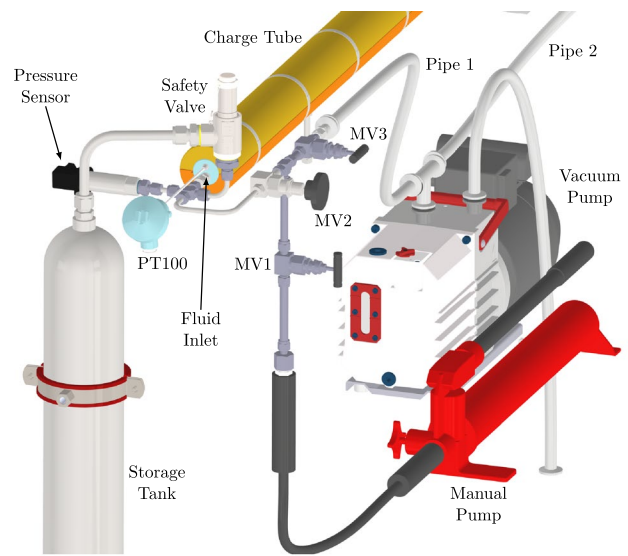
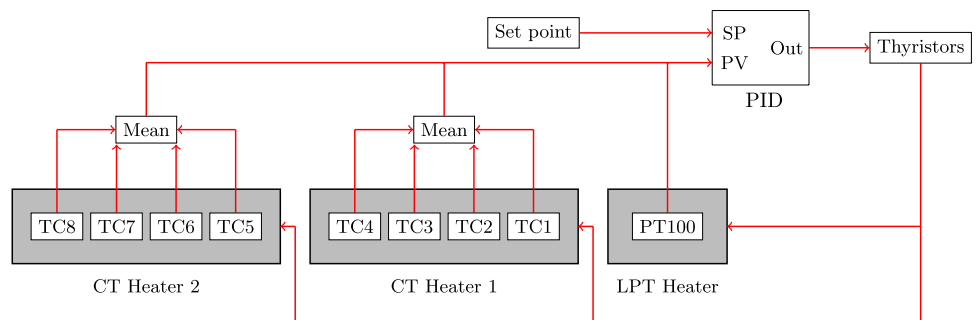


Fig. 7 Close-up of the inlet-side end of the ASTER

Fig. 6 Schematic of the temperature control logic. PV and SP in the PID block stand for process variable and set point, respectively



of the safety valve is connected to a collection tank with a volume of 4 ls to store the escaped fluid.

Four fast-response pressure transmitters tagged as PT1,..., PT4 (Kulite XTEH-10 L-190SM-300PSI-A) are flush mounted along the CT at distances of 1.2, 1.4, 1.6 and 1.8 m from the nozzle throat, respectively (see Fig. 2). These sensors feature a full scale of 21 bar and a bandwidth from 0 Hz to 250 kHz, and can withstand up to 500°C. The sensors are affected by significant drift of the calibration constant with temperature, but are suitable for recording fast-changing fluid pressure like that occurring in a shock tube. The 5-100 mV signals of the fast-response pressure sensors are amplified using a custom-built amplifier with a gain of 120 and are connected to the NI9222 module.

2.2 Experimental procedure

Prior to the experiments, a 3.3 mm thick borosilicate glass-disk of diameter 50 mm is positioned inside the LPT at the exit of the nozzle and the setup is vacuumed using a Pfeiffer Duo 5 M vacuum pump to remove all contaminants and gases from the apparatus. The vacuum pump is connected to the CT via pipe 1 and manual valves MV2 and MV3, and to the LPT via pipe 2 and manual valve MV4 (see Figs. 4 and 7).

The presence of oxygen and moisture dissolved in the working fluid or adsorbed on the surface of the containment metal are known to promote decomposition of organic compounds, thus also of siloxanes, at high temperature (Angelino and Invernizzi 1993; Colonna 1996; Calderazzi and Colonna 1997; Dvornic 2008; Keulen et al. 2018). Water dissolved in the working fluid is removed by letting the fluid sit in a container with 3 Å molecular sieve desiccants for several days. The presence of incondensable gases in the CT can also adversely affect the outcome of the experiments, because it affects the speed of sound and in general the propagation of waves. Since the CT is open and exposed to the atmosphere in between tests, gases can get adsorbed onto its inner walls. They are therefore removed by vacuuming the

CT multiple times as it is heated to the desired temperature prior to filling with D_6 .

Once the setup is evacuated, valves MV2, MV3 and MV4 are closed and the setup is sealed. The required volume of the fluid is estimated using the CT volume and the density of the fluid at the desired experimental conditions, computed using the best available thermodynamic model of the fluid (Colonna et al. 2019; Chandrasekaran 2023, Chapter 5). A HiForce HP110 hydraulic hand pump which has a total volume of 1 L and a stroke length of 250 mm, is connected to the CT via the manual valves MV1 and MV2. The carefully prepared working fluid is introduced into the CT using the hand pump by opening these valves.

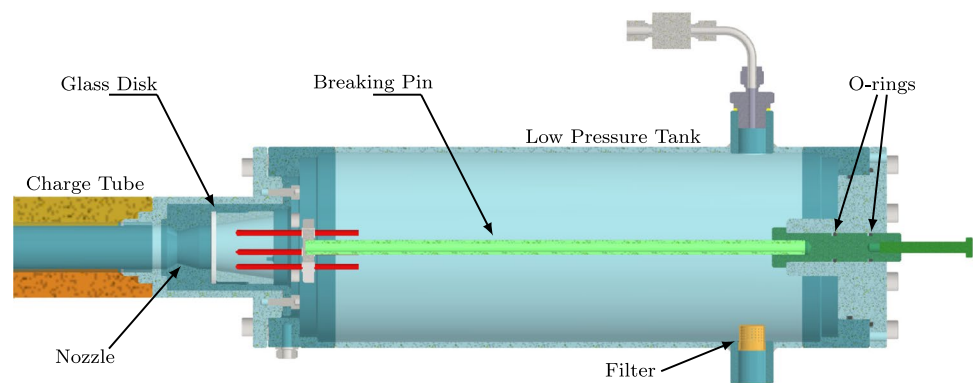
Once the charge tube is filled with the correct amount of fluid, it is heated by means of the blankets up to the set temperature. The heating process is controlled as described in Sect. 2.1. When the temperature within the charge tube has stabilized, the data acquisition of the signal from the high-frequency-response pressure transducers is started.

The breaking of the glass-disk is achieved by means of the breaking mechanism shown in Fig. 8. The breaking pin consists of six carbide twist drill bits each of 8.5 mm diameter attached to a 348 mm long stainless steel rod that is mounted on a base of length 140 mm. The end of the base protrudes outside of the LPT. Two Kalrez® O-rings on the base ensure that the working fluid does not leak during experiments. To initiate an experiment, the end of the breaking pin is hit with a hammer such that the glass shatters in the shortest possible time. Once the experiment is finished, the end-plate of the LPT is opened to remove the broken glass and a new glass-disk is placed. Although this mechanism requires opening the ASTER after each use, it allows for a quick and complete opening of the nozzle.

The speed of the wave is measured with a time-of-flight method, by correlating the pressure signals to obtain the time it takes to the wave to travel from one pressure transducer to the other and by knowing the distance between the transducers.

The working fluid that condenses in the LPT is extracted by opening manual valve MV5 at the bottom of the LPT,

Fig. 8 Vertical cross-section view of the LPT showing the glass-disk and the breaking pin assembly



see Figs. 4 and 8. A metallic filter placed within the LPT at the mouth of the outlet pipe ensures that glass pieces do not enter the outlet and block the flow. The fluid collected in the CT is removed when the setup is heated and vacuumed during the next experiments.

3 Facility characterization

A series of air tightness tests were performed to assess the leak rate of the facility. As explained in Sect. 2.2, it is of the utmost importance that leakages of air in the setup, especially at low pressure when air can enter the CT, are avoided. The tightness of the setup can be characterized with the average leak rate, defined as $LR = V\Delta P \cdot \Delta t^{-1}$, where V is the inner volume of the CT ($\sim 0.0022 \text{ m}^3$), and ΔP is the rise/drop in pressure measured after a time interval of Δt . At vacuum conditions, an inward LR of $2.2 \times 10^{-4} \text{ mbar l s}^{-1}$ was measured (air leaking into the system). Leakage tests at superatmospheric pressures conducted at different temperatures by filling the setup with air were consistently below $5 \times 10^{-4} \text{ mbar l s}^{-1}$ (air escaping the setup). This leak rate is lower than that measured for the FAST facility and reported by Mathijssen (2017). Moreover, in that case the same working fluid (96 % pure D_6 according to the gas chromatographic analysis provided by the supplier) showed no appreciable change of the fluid composition at high temperatures. The tightness degree of the ASTER is therefore deemed satisfactory for the envisaged experiments.

Rarefaction wave experiments in air were performed to demonstrate the correct operation of the setup, therefore the possibility of measuring wave propagation speeds at different locations along the charge tube. Figure 9 shows the temporal pressure measurements during an air rarefaction experiment whereby the initial thermodynamic state in the

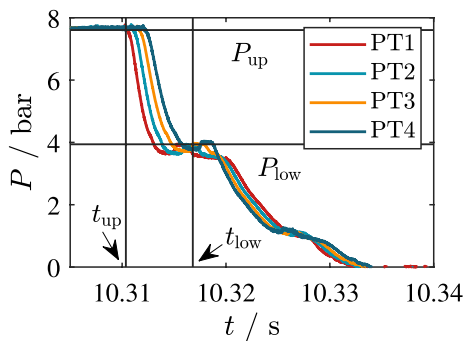


Fig. 9 Pressure as a function of time measured by the four sensors along the charge tube during an air expansion test. The initial thermodynamic state of air in the charge tube before the glass-disk was broken was set by a pressure of 7.6 bar and a temperature of 21°C. The bounds within which the time-of-flight method is applied are also shown

CT is given by a pressure of 7.67 bar and a temperature of 20.6°C, while the LPT is in vacuum conditions. The propagating initial rarefaction wave is seen as the large pressure drop from the CT state of 7.67 bar to approximately 4 bar in Fig. 9, which is set by the throat conditions in the choked nozzle. The subsequent drop in pressure corresponds to the reflected wave as it travels back into the CT. The order of the pressure signals are therefore reversed with respect to the initial pressure drop. This pattern in the pressure signals is repeated till the wave is completely dissipated.

The speed of the propagating wave in the CT at a given location is measured with the so-called *time-of-flight* (ToF) method. The pressure drop across the expansion wave at a given location is measured by the pressure sensors PT1, PT2, PT3 and PT4 placed 20 cm apart from each other, see Fig. 2. The wave speed w is then calculated as

$$w = \frac{L_T}{\Delta t}, \tag{2}$$

where L_T is the distance between two pressure sensors with the metal of the CT at temperature T , and Δt is the time it takes for the wave to propagate from the first to the second sensor. The distance L_T accounts for the thermal expansion of the metal of the charge tube and is estimated as

$$L_T = L_{T_0} [1 + \alpha(T - T_0)], \tag{3}$$

where L_{T_0} is the reference length between two sensor pairs (distance at the T_0 reference temperature), and $\alpha = 17.5 \times 10^{-6} \text{ K}^{-1}$ is the thermal expansion coefficient of the 316Ti stainless steel.

L_{T_0} is evaluated by measuring the propagation speed of a small amplitude wave in air for which accurate data are available in the literature, see, e.g., the articles of Wong (1986); Cramer (1993); Huang et al. (2002); Yavuz (2015). Therefore, by measuring the time delay Δt of arrival of the acoustic wave to the second sensor, the distance L_{T_0} between the two sensors can be computed according to Eq. (2) as

$$L_{T_0} = c_{\text{air, model}} \cdot \Delta t. \tag{4}$$

The measurement was conducted in dry air at 7.78 bar and 37°C, and the local speed of sound in these conditions was estimated using the reference multiparameter EoS model for air (Lemmon et al. 2013). Table 2 lists the distances between pressure sensor pairs computed with this method.

Table 2 Distances between the pressure sensors PT1, PT2, PT3 and PT4 (see Fig. 2) computed according to Eq. (4) at the T_0 reference temperature

	$c_{\text{air, model}} / \text{m s}^{-1}$	$L_{12, T_0} / \text{m}$	$L_{23, T_0} / \text{m}$	$L_{34, T_0} / \text{m}$
$T_0 = 37^\circ\text{C}$	351.99	0.201	0.201	0.198

In order to evaluate the time instant at which the wave passes over the sensor, each pressure signal is conditioned using a Gaussian-weighted moving average filter. This is followed by the identification of the section of the smoothed signal over which the ToF method can be applied. The upper and lower bounds of this section of the signal are defined as follows: the upstream bound is identified as the time instant, t_{up} , when the pressure deviates from the pressure of the initial state by more than 15 mbar. This is taken to be the head of the travelling rarefaction wave, and this pressure difference exceeds the level of the pressure fluctuations due to the signal noise. The downstream bound of the signal section, t_{down} , is chosen as the estimated time when the head of the wave reaches the end of the CT from the first sensor. To compute this time, the speed of sound, c , as predicted by the thermodynamic model at the experimental initial conditions is used. Therefore, it follows that

$$t_{down} = t_{up} + \frac{\Delta x}{c}, \tag{5}$$

where Δx is the distance between PT1 and the end of the CT (≈ 1.8 m). The relevant section of the signal then spans from P_{up} to P_{down} (see Fig. 9).

Figure 10 shows the computed wavespeed values w as a function of the drop in pressure ΔP across the wave. A theoretical curve of w obtained by subtracting the flow velocity from the soundspeed as a function of the pressure drop is also shown. The soundspeed is estimated using the ideal-gas thermodynamic model and assuming an isentropic expansion. The flow velocity is obtained by computing the Riemann invariant in the undisturbed state, which, in this simple wave, is constant (Thompson 1988). As expected for the case of ideal-gases, the model-predicted and the experimental wavespeeds show good accordance with each other.

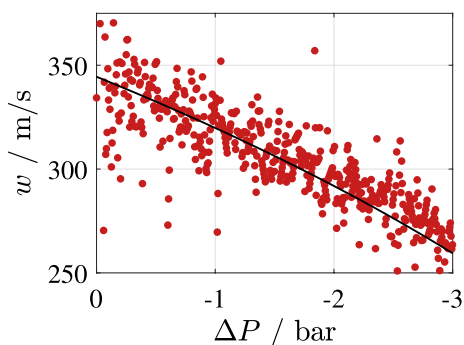


Fig. 10 Wavespeed estimates obtained with the time-of-flight method for expansion tests in air (red dots), and wavespeed estimated using ideal gas thermodynamic model (—).

The noise in the pressure signals, however, propagates into w resulting in the large scatter observed in Fig. 10.

Table 3 Relevant thermophysical properties of the working fluid D_6 (Colonna et al. 2008). MW is the molecular weight, P_c , T_c , and v_c are the estimated critical pressure, temperature and specific volume, respectively

	CAS Nr.	MW / (kg · kmol ⁻¹)	P_c / bar	T_c / °C	v_c / (m ³ · kg ⁻¹)
D_6	540-97-6	444.92	9.61	372.6	0.0036

4 D_6 rarefaction experiments

A series of rarefaction tests were performed with the aim of validating the possibility of measuring the speed of propagation of waves in the dense vapor of D_6 and estimating the local value of the fundamental derivative of gasdynamics Γ . D_6 was chosen as working fluid following the results of previous studies (Colonna and Rebay 2004; Colonna et al. 2007; Mathijssen et al. 2015) for its high thermal stability, low levels of both flammability and toxicity for humans, and the large size of negative- Γ region predicted by state-of-the-art thermodynamic models. D_6 is used in bulk quantities in the cosmetic industry. The primary properties of the pure fluid are summarized in Table 3. The fluid used in the tests was produced by Dow Corning. The gas-chromatography report accompanying the fluid states that it is 97.4% pure and its composition is shown in Table 4.

The initial thermodynamic states of the experiments are chosen based on the predictions of the best available thermodynamic model of the fluid (Colonna et al. 2008, 2019) and on the theory of nonideal compressible fluid dynamics (Guardone et al. 2024). Temperature and pressure were set such that the wave propagation can be expected to be different from classical, therefore nonideal and nonclassical. Table 5 lists the fluid initial states in terms of pressure and temperature, along with the corresponding calculated values of the fundamental derivative of gas dynamics, of the compressibility factor and of the speed of sound. Of the eight facility commissioning experiments, only two experiments (Test #1 and # 6) are discussed in Sects. 4.1 and 4.2 because the other experiments provided similar and coherent results. These are highlighted in Table 5. Figure 11 shows these thermodynamic thermodynamic chart of D_6 ; $T_r = T/T_c$ is

Table 4 Composition of the working fluid supply used in the experiments based on the gas-chromatography report provided by the manufacturer

	CAS Nr.	MW / (kg · kmol ⁻¹)	Mole fraction / %
D_6	540-97-6	444.92	97.374
D_5	541-02-6	370.77	1.667
D_7	107-50-6	519.07	0.458
D_4	541-05-9	222.46	0.066
D_3	556-67-2	296.64	0.039

Table 5 Some relevant thermodynamic properties of the dense vapor state of the fluid prior to eight rarefaction wave propagation experiments. The thermodynamic state was fixed by setting the pressure P_0 and the temperature T_0 . The other associated properties relevant for nonideal rarefaction experiments are the fundamental derivative of gasdynamics Γ , the compressibility factor Z , and the speed of sound c . Γ , Z and c are computed with a multiparameter EoS model (Colonna et al. 2008, 2019). Highlighted rows are experiments treated in Sects. 4.1 and 4.2

Test No.	P_0 /bar	T_0 /°C	Γ	Z	c /(m/s)
1	2.66	349.8	0.86	0.86	93.35
2	2.89	300.3	0.73	0.78	80.64
3	5.85	357.6	0.59	0.68	72.76
4	8.87	370.9	0.096	0.48	48.18
5	8.96	369.6	-0.052	0.46	43.08
6	9.33	372.1	-0.013	0.43	39.8
7	9.37	370.7	6	0.21	42.5
8	9.4	371.97	0.023	0.41	36.55

the reduced temperature and $s_r = s/s_c$ is the reduced entropy. Information regarding all the remaining experiments can be found in the PhD dissertation of Chandrasekaran (2023).

Prior to performing experiments aiming at generating and measuring nonclassical rarefaction wave propagation, tests were also conducted with the fluid in an initial thermodynamic state that is mildly nonideal to demonstrate the correct operation of the setup and to validate the time-of-flight (ToF) procedure to measure the wavespeed in challenging thermodynamic and fluid conditions. It is important to remark here that the thermodynamic model currently available is affected by large uncertainties, especially for the thermodynamic states of interest here, therefore dense vapor states at high reduced temperature and pressure.

4.1 Nonideal classical rarefaction waves propagation

The mildly nonideal thermodynamic region includes fluid states featuring values of the fundamental derivative Γ between 0.7 and 1 (see Fig. 11). With the fluid in such an initial thermodynamic state, it is expected that the wave propagation causes a change of all flow variables similar to those that would occur if the fluid state featured $\Gamma > 1$, therefore similar to a classical rarefaction, except for the soundspeed, which increases across an expansion. In this case, therefore, the process is classified as a nonideal classical rarefaction.

Figure 12 shows the temporal recordings of the dynamic pressure sensors related to Test # 1 (see, Table 5 and Fig. 11). The fast-response Kulite sensors suffer from significant drift in the offset. The application of the ToF method requires that the sensors correctly indicate the same pressure of the initial state, therefore their signals are scaled using the static pressure sensor reading as a reference prior

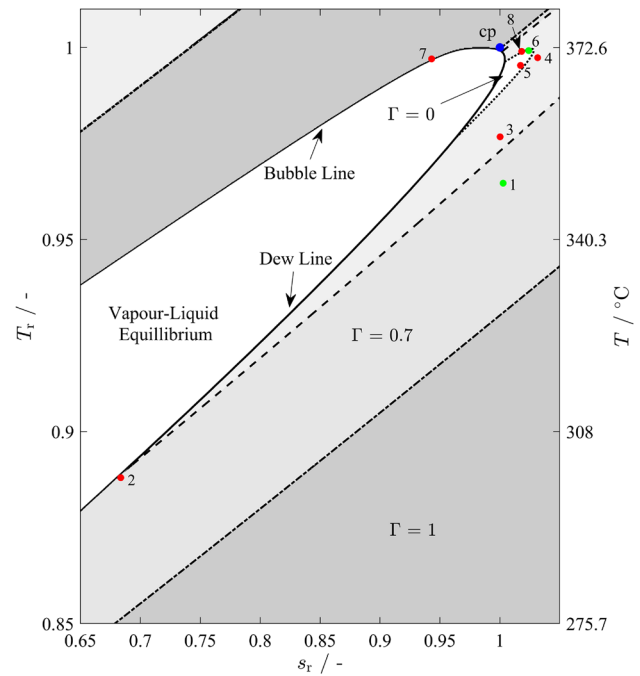
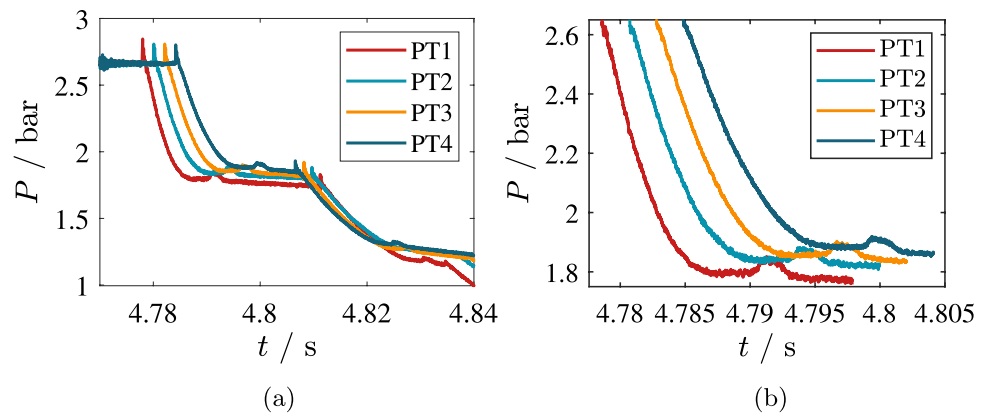


Fig. 11 $T_r - s_r$ diagram of D_6 . (●) Thermodynamic states at which rarefaction tests were performed, see Table 5. (●) Rarefaction tests #1 and # 6 discussed in Sect. 4.1 and Sect. 4.2. (—) saturation (or vapour-liquid equilibrium) line; (●) critical point. Few iso- Γ lines are also indicated. Data are calculated with the multiparameter EoS model for D_6 (Colonna et al. 2008, 2019)

to the experiment. Figure 12a shows the corrected pressure signals acquired during Test # 1. Furthermore, Fig. 12a puts into evidence a distinct peak at the leading edge of the wave, which also propagates with it. This peak is attributed to the almost instantaneous compression of the glass disk resulting from the impact of the hammer, which is subsequently transferred to the dense fluid vapor just before the disk shatters. The pressure signals display the propagation of the incident and the reflected rarefaction waves, as also observed in Fig. 9. Figure 12b displays the signal window of the filtered pressure recordings obtained through the procedure described in Sect. 3. The time-of-flight (ToF) method is applied to these filtered portions of the signals to estimate the wavespeed.

Figure 13a and b show the plot of the wave propagation speed as a function of the difference of the local pressure with the initial pressure, determined using the ToF method applied to the signals of pairs of pressure sensors. To limit the effect of the signal noise, a zero-phase, sixth order Butterworth digital filter is applied to the estimated wavespeed values. The plots also display the wave propagation speed calculated for comparison with the model valid for a shock-free isentropic flow expansion. Thermodynamic properties

Fig. 12 Test # 1: temporal pressure recordings of a nonideal classical rarefaction (see Table 5). **a** Dynamic pressure signals corrected for the offset drift using the static pressure measurement prior the experiment as the reference (see *Static Pressure Sensor* in Fig. 7). **b** Signal window of the filtered pressure recordings. This portion of the signals is used to compute the wavespeed using the time-of-flight method



are estimated with the multiparameter EoS model for D_6 (Colonna et al. 2008, 2019).

The measured wavespeed decreases monotonically as the pressure across the wave drops, as expected for these fluid thermodynamic conditions. The model-estimated wavespeed values are in relatively good agreement with the measured values as it can be expected if the fluid is in mildly nonideal thermodynamic states. The deviation between the measured and the model-predicted wavespeeds associated with $\Delta P \approx -0.6$ bar occurs at the tail of the wave ($P \approx 1.8$ bar in Fig. 12) where the signals flatten as the pressure reaches the throat pressure set by the choked nozzle.

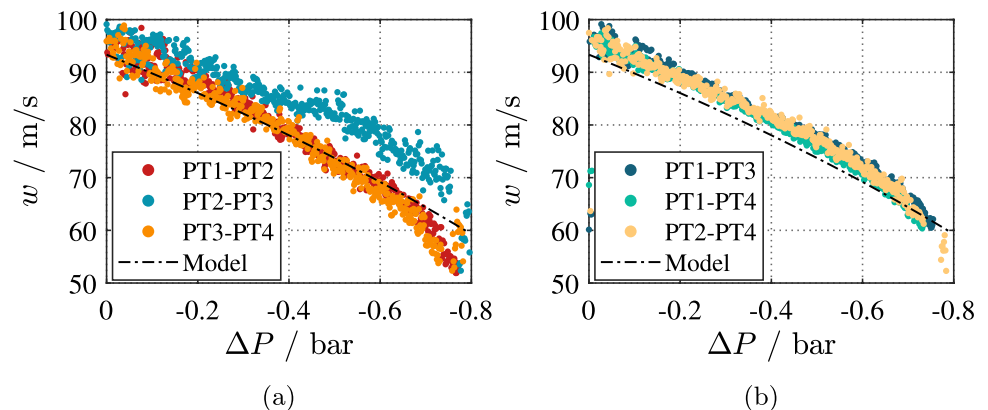
Interestingly, the wavespeeds estimated using adjacent sensors pairs (see Fig. 13a) are affected by much larger differences if compared to those obtained with non-adjacent sensor pairs (see Fig. 13b). A significant deviation from the calculated wavespeed values can be observed in Fig. 13a for those estimated using the values recorded by sensors PT2 and PT3. This discrepancy may be explained by considering that PT2 and PT3 are located on either side of the junction between the two thermal blankets covering the CT, therefore cold spots may be expected. A temperature gradient along the direction of the propagation of the wave, albeit small, makes the wave propagation model invalid.

4.2 Rarefaction wave propagation in dense vapor

The dense vapor thermodynamic region includes subcritical fluid states for which $Z < 1$. A subset of this region, in case the fluid molecule is sufficiently complex, includes states that feature negative values of Γ (refer to Fig. 11). Compressible flow processes involving $\Gamma < 0$ fluid states, only or partially, pertain, according to the current theory, to the realm of nonclassical gasdynamics. Nonclassical gasdynamic phenomena include rarefaction shock waves and isentropic compression fans. These phenomena have never been proved experimentally.

Data related to the initial thermodynamic state of the fluid for Test # 6 are reported in Table 5, and are plotted on a $T - s$ chart in Fig. 11. Figure 14 shows the sections of the pressure signal used to estimate the wavespeed using the ToF method. Compared to the pressure signals of Test # 1, the pressure recordings exhibit a steeper and larger drop. Additionally, the signals display an abrupt change of the pressure gradient occurring close to the head of the wave. This abrupt change appears only in the pressure signals obtained during experiments performed in dense vapor gasdynamic conditions, and is absent during tests in both ideal gas and with D_6 in the mildly nonideal gasdynamic region (see Sects. 3 and 4.1). This suggests that this signal feature is possibly related to a

Fig. 13 Test # 1 (see Table 5): wavespeed estimates of a nonideal classical rarefaction obtained with the time-of-flight method using the pressure signals of **a** adjacent and **b** non-adjacent sensor pairs (see Fig. 2)



dense-vapor effect rather than one caused by an interaction of the fluid with a mechanical component, such as the breaking pin or a geometric irregularity of the CT.

Figure 15a and b shows the variation of the estimated wavespeed as a function of the pressure drop, computed starting from the pressure values recorded by adjacent and non-adjacent sensor pairs, respectively. In contrast to results obtained with the data recorded during Test # 1 (see Fig. 13), the wavespeed values depart significantly from the values computed with the model. Prior to the abrupt change in the pressure gradient seen in Fig. 14, the wavespeed decreases with decreasing ΔP , which is characteristic of a classical expansion (see Sect. 4.1). This could possibly indicate that the local value of Γ for the CT thermodynamic conditions, in contrast to the model predicted value reported in Table 5, is positive, and the thermodynamic state lies above the $\Gamma < 0$ region (see Fig. 11). Past the abrupt pressure change, i.e., for $\Delta P < -0.4$ bar, the wavespeed computed from measured temporal pressure values remains nearly constant and independent of the pressure drop until the ΔP is ≈ -1 bar. Subsequently, the wavespeed reduces again with the pressure drop.

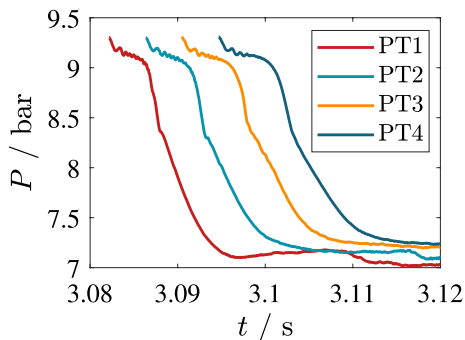
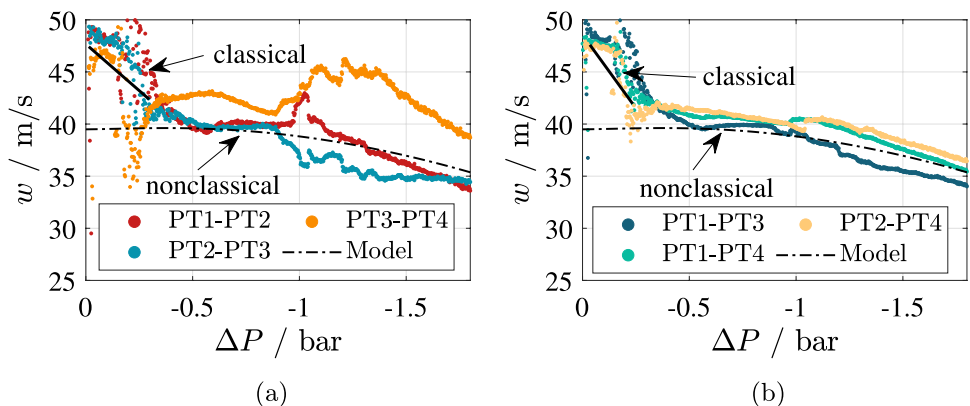


Fig. 14 Test # 6: Pressure signal window of the filtered pressure recordings related to a possibly nonclassical rarefaction (see Table 5). This portion of the pressure recordings is used to compute the wavespeed using the time-of-flight method

Fig. 15 Test # 6 (see Table 5): wavespeed estimates of a possibly nonclassical rarefaction obtained with the time-of-flight method using the pressure signals of sensors **a** adjacent and **b** non-adjacent sensor pairs (see Fig. 2)



This variation of the wavespeed maybe indicative of a rarefaction wave that originates from a thermodynamic state outside of the negative Γ region ($0 < \Delta P \lesssim -0.3$ bar), thus classical, and that evolves as a nonclassical rarefaction shock wave with the fluid in thermodynamic states featuring $\Gamma < 0$ (for ΔP between -0.5 bar and -1 bar). As the wave evolves further into fluid states that again feature $\Gamma > 0$, i.e., for $\Delta P > -1$ bar, the rarefaction continues in the classical regime. This evolution of the waves is qualitatively depicted in Fig. 16.

4.3 Estimation of Γ along the dense vapor rarefaction waves propagation

Following Thompson (1971), the fundamental derivative of gas dynamics Γ is related to the local wave speed, density, and soundspeed through

$$\Gamma = \zeta \left. \frac{dw}{dp} \right|_s, \tag{6}$$

where $\zeta = \rho c$ is the *acoustic impedance*. The value of dw/dp can be obtained by numerically differentiating the wave speed evaluated using the ToF method. Since ρ and c are not directly measured during the experiment, it is not possible to obtain the value of Γ as a function of the pressure drop across the wave solely from experimental data. However, since both ρ and c are positive quantities, the sign of dw/dp is also the sign of Γ , and $dw/dp = 0$ across a rarefaction shock wave. This evaluation would allow to ascertain if thermodynamic states featuring negative values of Γ exist. Moreover, if the value of dw/dp is constant and close to zero, this may indicate that a nonclassical shock has formed in the flow field.

Figure 17 displays a chart of the derivative of the wavespeed with respect to pressure drop across the wave, computed using the pressure signals recorded by adjacent (PT1-PT2) and non-adjacent (PT1-PT4) sensor pairs during Test # 1. This wavespeed derivative is calculated numerically

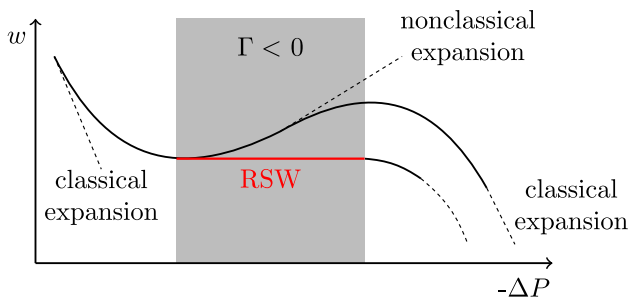


Fig. 16 Qualitative representation of the variation of wavespeed with the pressure drop across a wave undergoing an unsteady expansion in which the fluid thermodynamic states feature $\Gamma < 0$ for part of the process. The results of Fig. 15 may be interpreted in the light of such variation as a classical expansion evolving into a rarefaction shock, which subsequently becomes again a classical rarefaction

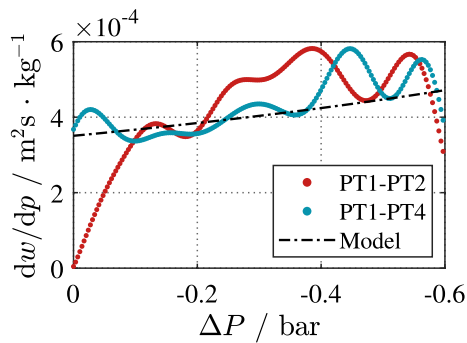
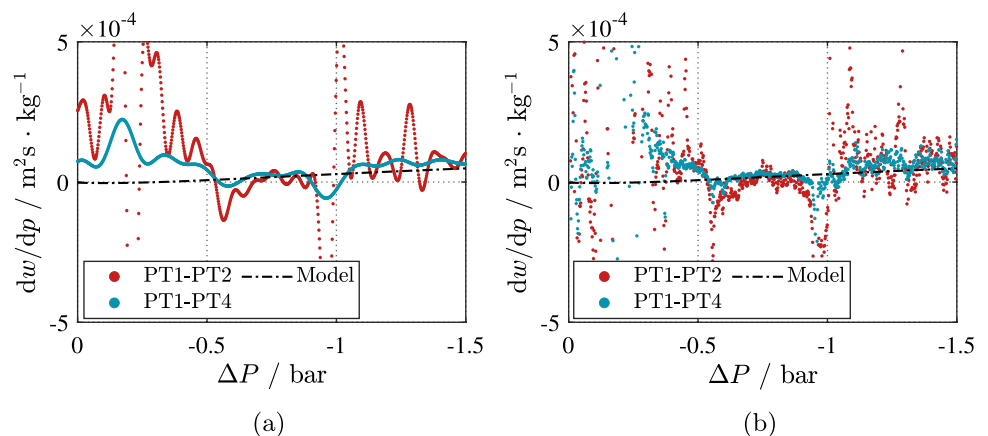


Fig. 17 Test #1: derivative of the wave speed with respect to pressure drop computed with values recorded by sensor pairs PT1-PT2 and PT1-PT4. Values of the wave speed computed with Eq. (6) and properties estimated with the EoS thermodynamic model are shown as a black dashed line

with a central differences scheme, except for values at the boundaries of the domain, for which single-sided differences are adopted. The fluctuations of the values of dw/dp are most likely residual low wavenumber oscillations which

Fig. 18 Test # 6: derivative of the wave speed with respect to pressure computed with values recorded by sensor pairs PT1-PT2 and PT1-PT4. The derivatives are computed using **a** filtered wavespeed measurements and **b** unfiltered wavespeed measurements. Values of the wave speed computed with Eq. (6) and properties estimated with the EoS thermodynamic model are shown as a black dashed line



fall below the cutoff wavenumber of the filter and are then amplified by the differentiation. Figure 17 also shows the wavespeed derivative values computed with fluid property estimates provided by the multiparameter EoS model.

Similar to what can be observed in Fig. 13a and b, the estimate of dw/dp computed using the pressure signals recorded by PT1-PT4 is less affected by oscillations and values are more in agreement with those computed with the model. Moreover, dw/dp is positive and increases with the pressure drop associated with the wave propagation, as theoretically predicted for a classical rarefaction in which the fluid thermodynamic states are mildly nonideal.

Figure 18 shows the plot of the derivative of the wavespeed as a function of the pressure drop across the wave, obtained numerically in the same way as that reported in the chart of Fig. 17, computed using the values acquired by sensor pairs PT1-PT2 and PT1-PT4 during Test # 6. Also in this case, and for the same reason, oscillations are evident, especially close to the head and tail of the wave. However, it is clearly evident that for $-0.5 \leq \Delta P \leq -1$ bar, the average of the values of dw/dp is nearly constant, and this is consistent with the observations provided in relation to Fig. 15, therefore consistent with the possibility that a rarefaction shock wave has formed. Beyond $\Delta P \approx -1$ bar, dw/dp once again increases and follows the trend of the values computed with the wave propagation model.

Figure 18b shows the plot of the values of the derivative estimated using the unfiltered pressure signals acquired by same two sensor pairs as in Fig. 18a. The average of $dw/dp \approx 0$ for values of the pressure drop across the wave between -0.5 bar and -1 bar. Since according to theory, dw/dp and Γ are constant and zero across a RSW, these values of dw/dp obtained from the temporal pressure measurements shown in Fig. 15a and b suggest the occurrence of nonclassical gasdynamic effects, and even possibly the propagation of a rarefaction shock wave.

5 Conclusions

A novel shock tube facility for the study of nonideal and nonclassical gasdynamic flows has been designed, realized and successfully commissioned at Delft university of Technology. This facility, called the asymmetric shock tube for experiments on nonideal rarefaction waves (ASTER), is specifically designed to generate and detect the nonclassical formation of rarefaction shock waves (RSWs) or to measure the propagation speed of classical nonideal rarefaction waves in fluids made of complex organic molecules. The ASTER can withstand pressures and temperatures of up to 15 bar and 400°C. The fluid used for commissioning and to perform the first experiments is siloxane D_6 . A nonclassical gasdynamic experiment is conceived to detect accelerating rarefaction waves by measuring their speed of propagation. According to theory, if rarefaction waves accelerate over isentropic expansion, they are bound to form a rarefaction shock wave which moves at a speed that is higher than the local speed of sound of the fluid. The existence of nonclassical gasdynamic phenomena has not been experimentally proven yet.

Initially, the facility has been characterized by demonstrating the possibility to measure the speed of propagation of expansion waves in air. Successively, in order to commission the ASTER, a series of rarefaction tests in D_6 were performed. The initial thermodynamic states were selected based on the prediction provided by the best available thermodynamic model with thermodynamic properties ranging from mildly nonideal to the strongly nonideal. The speed of the propagating rarefaction waves was estimated with a time-of-flight (ToF) method applied to the values of pressure recorded by fast-response sensors placed along the charge tube. These wavespeed measurements were used to derive the sign of the fundamental derivative of gasdynamics, Γ , or to ascertain if Γ may be zero or negative over some portions of the propagating rarefaction wave.

The experiments performed with the fluid in an initial thermodynamic state that is predicted to feature $\Gamma < 0$ revealed a wave propagation pattern that qualitatively differs from that of tests performed at lower pressures and temperatures. Notably, the wave speed does not exhibit a monotonic decrease with the pressure drop across the wave. Instead, it remains nearly constant within specific ranges of negative ΔP across the wave, possibly indicating the formation of a nonclassical rarefaction shock wave in the flow field. The temporal pressure recordings also allow to numerically evaluate the variation of dw/dp with ΔP , which is bound to feature the same sign of Γ according to theory (if $dw/dp = 0$, then $\Gamma = 0$). Calculated values of dw/dp that on average are approximately zero for portions of the pressure signal further support the possibility of

the existence of a rarefaction shock wave in the expanding flow.

In order to prove the existence of nonclassical gasdynamic phenomena, a more thorough investigation of rarefaction waves propagating in dense and close-to-critical vapor states is required. It is envisaged that the ability to set precise initial conditions for experiments will be enhanced, and the repeatability of experiments will be proven. In addition, it is desirable that the accuracy and reliability of the available thermodynamic model of D_6 is improved, especially for thermodynamic states close to the vapor-liquid equilibrium state.

With a more accurate thermodynamic model, it would be possible to set the initial state of the experiments based on the calculation of the state that maximizes the desired nonclassical gasdynamic effect, namely the acceleration of rarefaction waves and the strength of the rarefaction shock wave.

Given that the density of vapor and liquid are very similar close to the critical point, and that thermodynamic models predict that a set of vapor-liquid equilibrium states close to the critical point also feature negative Γ , nonclassical wave propagation experiments with the process entirely or partially occurring with the fluid in saturated conditions are also possible and relevant. Additionally, it would also be important to assess the impact of impurities in the fluid sample on rarefaction propagation and soundspeed. The fluid sample could be purified if necessary.

The availability of accurate soundspeed data related to dense vapor thermodynamic states is important to not only verify the formation of RSWs but, more importantly, also for the improvement of thermodynamic property models. The ASTER was operated also for preliminary measurements of the soundspeed in D_6 at various thermodynamic states. The results demonstrated that the experimental soundspeeds were consistently higher than the predictions of the thermodynamic model, with deviations up to 8.6% for states within the dense-vapor thermodynamic region. Further experiments to measure the soundspeed, especially at high reduced pressures and temperatures, are planned to support the optimization and improvement of the thermodynamic models for siloxane D_6 . The ASTER could be used to provide this type of experimental information for other complex organic molecules.

Author Contributions NC, BM and PC conceptualized the research project and designed the experimental setup. NC and TM constructed the setup and conducted the experiments. NC processed the data, prepared the figures and the original draft of the manuscript. TM, BM, CF and PC reviewed and edited the manuscript. CF contributed to planned updates to the facility and to ongoing and upcoming experiments. PC acquired the funding and the resources for the study.

Funding This research has been supported by the Applied and Engineering Sciences Division (TTW) of the Dutch Organization for

Scientific Research (NWO), Technology Program of the Ministry of Economic Affairs, Grant No. 15837.

Declarations

Conflict of interest The authors declare no competing financial or non-financial interests.

Open Access This article is licensed under a Creative Commons Attribution 4.0 International License, which permits use, sharing, adaptation, distribution and reproduction in any medium or format, as long as you give appropriate credit to the original author(s) and the source, provide a link to the Creative Commons licence, and indicate if changes were made. The images or other third party material in this article are included in the article's Creative Commons licence, unless indicated otherwise in a credit line to the material. If material is not included in the article's Creative Commons licence and your intended use is not permitted by statutory regulation or exceeds the permitted use, you will need to obtain permission directly from the copyright holder. To view a copy of this licence, visit <http://creativecommons.org/licenses/by/4.0/>.

References

- Angelino G, Invernizzi C (1993) Cyclic methylsiloxanes as working fluids for space power cycles. *J Sol Energy Eng* 115(3):130–137. <https://doi.org/10.1115/1.2930039>
- Borisov AA, Borisov AA, Kutateladze SS et al (1983) Rarefaction shock wave near the critical liquid-vapour point. *J Fluid Mech* 126:59–73. <https://doi.org/10.1017/s002211208300004x>
- Calderazzi L, Colonna P (1997) Thermal stability of R-134a, R-141b, R-131i, R-7146, R-125 associated with stainless steel as a containing material. *Int J Refrigeration-revue Int Du Froid* 20(6):381–389. [https://doi.org/10.1016/s0140-7007\(97\)00043-1](https://doi.org/10.1016/s0140-7007(97)00043-1)
- Chandrasekaran NB (2023) Nonclassical gasdynamics: theory and experiments on nonlinear wave propagation in BZT fluids. PhD thesis, Delft University of Technology. <https://doi.org/10.4233/UUID:65D578CE-B904-466F-A57E-4086DBEE4A98>
- Chandrasekaran NB, Mercier B, Colonna P (2021) Nonlinear wave propagation in dense vapor of Bethe-Zel'dovich-Thompson fluids subjected to temperature gradients. *Phys Fluids*. <https://doi.org/10.1063/50063226>
- Colonna P (1996) Fluidi di lavoro multi componenti per cicli termodinamici di potenza (Multicomponent working fluids for power cycles). PhD thesis, Politecnico di Milano
- Colonna P, Rebay S (2004) Numerical simulation of dense gas flows on unstructured grids with an implicit high resolution upwind Euler solver. *Int J Numer Meth Fluids* 46(7):735–765. <https://doi.org/10.1002/fld.762>
- Colonna P, Guardone A, Nannan NR (2007) Siloxanes: a new class of candidate Bethe-Zel'dovich-Thompson fluids. *Phys Fluids*. <https://doi.org/10.1063/12759533>
- Colonna P, Nannan NR, Guardone A (2008) Multiparameter equations of state for siloxanes: [(CH₃)₃-Si-O/2]₂-[O-Si-(CH₃)₂]_i=1,...,3, and [O-Si-(CH₃)₂]₆. *Fluid Phase Equilibria* 263(2):115–113. [10.1016/j.fluid.2007.10.001](https://doi.org/10.1016/j.fluid.2007.10.001)
- Colonna P, van der Stelt TP, Guardone A (2019) FluidProp (Version 3.1): a program for the estimation of thermophysical properties of fluids. <http://www.asimptote.nl/software/fluidprop>, a computer program since 2004
- Cramer O (1993) The variation of the specific heat ratio and the speed of sound in air with temperature, pressure, humidity, and CO₂ concentration. *J Acoust Soc Am* 93(5):2510–2516. <https://doi.org/10.1121/1.405827>
- Dvornic PR (2008) Silicon compounds: silanes and silicones. Gelest Inc., Morrisville, PA, chap High temperature stability of polysiloxanes, pp 419–431
- Ferguson S (2001) Dense gas shock tube: Design and analysis. PhD thesis, University of Colorado, Boulder
- Furukawa T, Aochi T, Sasoh A (2007) Expansion tube operation with thin secondary diaphragm. *AIAA J* 45(1):214–217. <https://doi.org/10.2514/1.23846>
- Gaetani P, Guardone A, Persico G (2008) Shock tube flows past partially opened diaphragms. *J Fluid Mech* 602:267–286. <https://doi.org/10.1017/s0022112008000815>
- Guardone A, Zamfirescu C, Colonna P (2009) Maximum intensity of rarefaction shock waves for dense gases. *J Fluid Mech* 642:127–146. <https://doi.org/10.1017/s0022112009991716>
- Guardone A, Colonna P, Pini M et al (2024) Nonideal compressible fluid dynamics of dense vapors and supercritical fluids. *Annu Rev Fluid Mech* 56(1):241–269. <https://doi.org/10.1146/annurev-fluid-120720-033342>
- Head AJ (2021) Novel experiments for the investigation of non-ideal compressible fluid dynamics: the ORCHID and first results of optical measurements. PhD thesis. <https://doi.org/10.4233/UUID:A3B03976-2DF6-435C-B7DF-1505718FCD3A>
- Houas L, Jourdan G, Schwaederlé L et al (2003) A new large cross-section shock tube for studies of turbulent mixing induced by interfacial hydrodynamic instability. *Shock Waves* 12(5):431–434. <https://doi.org/10.1007/s00193-002-0173-y>
- Huang KN, Huang CF, Li YC et al (2002) High precision, fast ultrasonic thermometer based on measurement of the speed of sound in air. *Rev Sci Instrum* 73(11):4022–4027. <https://doi.org/10.1063/1.1510576>
- Keulen L, Gallarini S, Landolina C et al (2018) Thermal stability of hexamethyldisiloxane and octamethyltrisiloxane. *Energy* 165:868–876. <https://doi.org/10.1016/j.energy.2018.08.057>
- Lemmon E, Huber M, McLinden M (2013) Nist standard reference database 23: reference fluid thermodynamic and transport properties-refprop, version 9.1. https://tsapps.nist.gov/publication/get_pdf.cfm?pub_id=912382
- Mathijssen T (2017) Experimental observation of non-ideal compressible fluid dynamics. PhD thesis, Delft University of Technology. <https://doi.org/10.4233/UUID:147F6475-1B33-4A5A-9E65-ABE63A3865FF>
- Mathijssen T, Gallo M, Casati E et al (2015) The flexible asymmetric shock tube (FAST): a Ludwig tube facility for wave propagation measurements in high-temperature vapours of organic fluids. *Exp Fluids*. <https://doi.org/10.1007/s00348-015-2060-1>
- Mercier B, Chandrasekaran NB, Colonna P (2023) Speed of sound measurements in dense siloxane d6 vapor at temperatures up to 645 K by means of a new prismatic acoustic resonator. *J Chem Eng Data* 68(3):561–573. <https://doi.org/10.1021/acs.jced.2c00725>
- Nambiar GK, Sriram M, Dharanidhar M et al (2017) Design and fabrication of hand operated mini shock tube. *IOP Conf Ser Mater Sci Eng* 225:01202. <https://doi.org/10.1088/1757-899x/225/1/012025>
- Nannan NR (2009) Advancements in nonclassical gasdynamics. PhD thesis, Delft University of Technology
- Nannan NR, Guardone A, Colonna P (2013) On the fundamental derivative of gas dynamics in the vapor-liquid critical region of single-component typical fluids. *Fluid Phase Equilib* 337:259–273. <https://doi.org/10.1016/j.fluid.2012.09.017>
- Thompson P (1988) Compressible-fluid dynamics. *Adv Eng Ser*. https://books.google.nl/books?id=_btCmgEACAAJ
- Thompson PA (1971) A fundamental derivative in gasdynamics. *Phys Fluids* 14(9):1843–1849. <https://doi.org/10.1063/1.1693693>

- Tranter RS, Brezinsky K, Fulle D (2001) Design of a high-pressure single pulse shock tube for chemical kinetic investigations. *Rev Sci Instrum* 72(7):3046–3054. <https://doi.org/10.1063/1.1379963>
- Wong GSK (1986) Speed of sound in standard air. *J Acoust Soc Am* 79(5):1359–1366. <https://doi.org/10.1121/1.393664>
- Yavuz A (2015) Measuring the speed of sound in air using smartphone applications. *Phys Educ* 50(3):281. <https://doi.org/10.1088/0031-9120/50/3/281>

Publisher's Note Springer Nature remains neutral with regard to jurisdictional claims in published maps and institutional affiliations.